# Characterization of Cardiac Repolarization Response to Heart Rate Changes Provoked by a Tilt Test

Julia Ramírez[1,2], Ana Mincholé[2,1], Pablo Laguna[1,2], Esther Pueyo[2,1]

[1] Communications Technology Group (GTC), Aragón Institute of Engineering Research (I3A), IIS Aragón, Universidad de Zaragoza, Zaragoza, Spain
[2] CIBER - Bioingeniería, Biomateriales y Nanomedicina, Spain

## Abstract

*In predicting the risk of suffering from ventricular arrhythmias, the dynamics of QT and T-peak-to-T-end ($T_{pe}$) intervals after changes in heart rate (HR) provide richer information than their values themselves. In this study, QT/RR and $T_{pe}$/RR dynamics were investigated. Electrocardiogram (ECG) recordings of healthy subjects were analyzed during a head-up tilt test. ECGs were delineated using multi-lead (ML) and single-lead (SL) techniques and the QT and $T_{pe}$ intervals series were obtained. QT/RR and $T_{pe}$/RR dynamics were modeled using a nonlinear system, from which the time constant of adaptation $t_{90}$ was derived. QT/RR dynamics is similar using SL or ML delineation, with adaptation times being: $t_{90}^{\text{SL}}$ [s] = 49.7 +/- 29.0, $t_{90}^{\text{ML}}$ [s] = 47.1 +/- 20.1. The $T_{pe}$ interval responded more abruptly to HR when calculated using SL as compared to ML. Consequently, $T_{pe}$/RR dynamics were characterized by different adaptation time constants depending on whether SL or ML was used: $t_{90}^{\text{SL}}$ [s] = 25.6 +/- 37.3, $t_{90}^{\text{ML}}$ [s] = 56.4 +/- 48.3. QT dynamics can be invariantly characterized using either SL or ML delineation, while $T_{pe}$ dynamics are highly sensitive to the delineation method. Differences arise from the way SL and ML delineation are affected by T-wave loop rotation. Care should be taken when electrophysiological interpretation is provided to measurements obtained from one or the other delineation methods.*

## 1. Introduction

Clinical and experimental studies have suggested that abnormalities of ventricular repolarization play a role in the genesis of ventricular arrythmias [1]. The QT interval of the electrocardiogram (ECG) is the most extensively used index of repolarization, but other ECG indices related to the T wave have been proposed in the last years, including the interval between the T wave peak and the T wave end ($T_{pe}$) [2]. The $T_{pe}$ interval is generally accepted to reflect differences in the time for completion of repolarization of different ventricular regions and has been proposed

as a measure of dispersion of repolarization [3]. Changes in this interval have been linked to alterations in spatial dispersion of repolarization that may be prognostic of arrythmic risk under a variety of conditions [4]. Repolarization indices such as the QT interval or the $T_{pe}$ interval depend on heart rate (HR) [5, 6] and such a dependence has also been related to arrythmic risk [7]. In this paper QT and $T_{pe}$ interval responses to HR changes are characterized, with those intervals delineated using both single-lead (SL) and multi-lead (ML) techniques.

## 2. Materials and methods

### 2.1. Materials

ECG recordings from a database acquired at the University of Zaragoza for the study of the autonomic nervous system (ANS-UZ) were analyzed. Recordings were obtained from 15 healthy subjects (11 males, 4 females) with no previous medical history related to cardiovascular diseases and with a mean age of $28.5 \pm 2.8$ years. Each recording consists of 8 ECG leads, sampled at 1000 Hz, acquired during a 13-min head-up tilt test (4-min supine, 5-min at $70°$, 4-min supine).

### 2.2. Methods

#### 2.2.1. Signal preprocessing

Preprocessing of the ECG signals includes low pass filtering at 40 Hz to remove electric and muscle noise and cubic splines interpolation for baseline wander removal.

#### 2.2.2. Repolarization indices

QT and $T_{pe}$ intervals were computed using both SL and ML delineation techniques.

- **Single-Lead delineation**
– **Selection of lead with the highest signal-to-noise ratio (SNR)**: In each subject, the lead with the highest SNR, estimated as the maximum T-wave amplitude over the root mean square value of the high-frequency noise (above 25 Hz) of the interval from the offset of the QRS complex to the onset of the P-wave is selected. In this database, leads

V2, V3 or V4 were in all the subjects the leads with the highest SNR [6].

– **SL delineation and beat selection**: ECG delineation was performed using a wavelet-based delineator [8]. Beat selection was performed, removing those beats where any of the marks corresponding to T-wave onset ($n_{T_{on}}^{\mathrm{SL}}$), T-wave peak ($n_{\mathrm{T}}^{\mathrm{SL}}$), T-wave offset ($n_{T_{off}}^{\mathrm{SL}}$) or QRS-complex onset ($n_{QRS_{on}}^{\mathrm{SL}}$) was missing.

– **Calculation of $y_{\mathrm{QT}}^{\mathrm{SL}}[i]$ and $y_{T_{pe}}^{\mathrm{SL}}[i]$ series**: For each beat $i$, the QT interval was computed as the time interval between QRS-complex onset and T-wave offset:

$$y_{\mathrm{QT}}^{\mathrm{SL}}[i] = (n_{T_{off}}^{\mathrm{SL}}[i] - n_{QRS_{on}}^{\mathrm{SL}}[i])T_s. \tag{1}$$

where $n_{T_{off}}^{\mathrm{SL}}[i]$ and $n_{QRS_{on}}^{\mathrm{SL}}[i]$ are the samples corresponding to T-wave offset and QRS-complex onset temporal marks, respectively, and $T_s$ is the sampling period ($T_s = 1$ ms).

The $T_{pe}$ interval was computed as the time interval between T-wave peak and T-wave offset:

$$y_{T_{pe}}^{\mathrm{SL}}[i] = (n_{T_{off}}^{\mathrm{SL}}[i] - n_{\mathrm{T}}^{\mathrm{SL}}[i])T_s \tag{2}$$

where $n_{\mathrm{T}}^{\mathrm{SL}}[i]$ is the sample related to T-wave peak.

• **Multi-Lead delineation**

ML delineation was performed over orthogonal leads (X, Y and Z) obtained from Dower's inverse matrix.

– **Computation of orthogonal signals**: Three orthogonal leads x[n], y[n] and z[n] were obtained by multiplying the eight standard leads with Dower's inverse matrix, $\mathbf{D}^{-1}$. The transformation equation is:

$$\mathbf{Y} = \mathbf{D}^{-1}\mathbf{X} \tag{3}$$

where $\mathbf{Y}$ represents the matrix that contains, columnwise, the three orthogonal leads and $\mathbf{X}$ is the matrix with the eight standard leads (I, III, V1, V2, V3, V4, V5 and V6).

– **ML delineation and beat selection**: ML delineation was applied to the three orthogonal leads obtained from equation (3). The 3D T-wave loop built from those leads was projected over the direction with the highest SNR in the interval of interest for delineation of T wave onset, peak or offset, and, therefore, optimal to be delineated. This method was applied on a beat-to-beat basis, taking into account that the optimal direction varies depending on whether onset, peak or offset is being delineated [8].

– **Calculation of $y_{\mathrm{QT}}^{\mathrm{ML}}[i]$, $y_{T_{pe}}^{\mathrm{ML}}[i]$ and $y_{T_c'}^{\mathrm{ML}}[i]$ series**: $y_{\mathrm{QT}}^{\mathrm{ML}}[i]$ and $y_{T_{pe}}^{\mathrm{ML}}[i]$ series were computed as in equations (1) and (2), but using the marks obtained from the ML delineation. Additionally, $y_{T_c'}^{\mathrm{ML}}[i]$ series was computed to assess differences in T-wave morphology between leads. $y_{T_c'}^{\mathrm{ML}}[i]$ series has been proposed as a measure of spatial dispersion of repolarization [9], which can be interpreted as the beat-to-beat ratio between the minor axis ($\lambda_2$) and the major one ($\lambda_1$) of the T-wave loop. Previous studies have associated heterogeneous repolarization with increments in $\lambda_2$

and, correspondingly, more circular loops [10]. $y_{T_c'}^{\mathrm{ML}}[i]$ series was computed as the ratio between the second and the first eigenvalue from correlation matrix $\hat{\mathbf{R}}_i$ [9]:

$$y_{T_c'}^{\mathrm{ML}}[i] = \frac{\lambda_2[i]}{\lambda_1[i]}, \tag{4}$$

with $\hat{\mathbf{R}}_i$ computed as

$$\hat{\mathbf{R}}_i = \mathbf{X}_i\mathbf{X}_i^T, \tag{5}$$

where $i$ represents beat index and $\mathbf{X}_i$ is the matrix that contains in its columns the T-wave complex of the three orthogonal leads (Nx3 matrix) for each i-$th$ beat.

Once the series were obtained, either using SL or ML delineation, a Median Absolute Deviation filter was used to remove possible outliers due to bad quality of the recorded signals or to the delineation procedure.

### 2.2.3. Repolarization adaptation to heart rate changes

Once the interval series were obtained, a series vector $\mathbf{y}_s$, was introduced, where "s" represents either QT or $T_{pe}$ intervals. The model shown in Fig. 1 was used to characterize the dependence of QT or $T_{pe}$ on RR [7]. The input $x_{\mathrm{RR}}[i]$ and output $y_s[i]$ of the system denote the RR and "s" series of each recording after interpolation and resampling to a sampling frequency of $F_m = 1$ Hz.
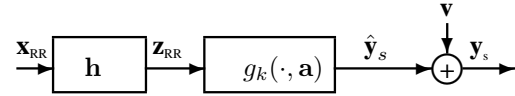


Figure 1. Block diagram describing the RR to "s" ("s" being QT or $T_{pe}$ intervals) relationship, consisting of a time invariant FIR filter (impulse response **h**) and a nonlinear function $g_k(\cdot, \mathbf{a})$.

Impulse response $\mathbf{h} = [h[1], ..., h[N]]^T$ includes information about the memory of the system, that is, a characterization of the influence of a history of previous RR intervals on each "s" measurement. Therefore, $z_{\mathrm{RR}}[i]$ represents a surrogate of $x_{\mathrm{RR}}[i]$ with the memory effect of "s" compensated for. The length N of vector **h** was set to 150 samples. The function $g_k(\cdot, \mathbf{a})$, dependent on the parameter vector $\mathbf{a} = [a(0), a(1)]^T$, represents the relationship between the RR interval and the "s" interval once the memory effect has been compensated for.

The optimum values of the FIR filter response **h**, vector **a**, and function $g_k$ are searched for by minimizing the difference between the estimated output $\hat{y}_s[i]$ and the system output $y_s[i]$, for each subject independently using the whole recording.
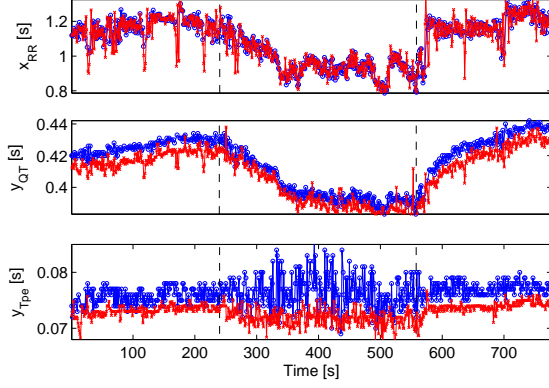
Figure 2. $x_{\text{RR}}[i]$, $y_{\text{QT}}[i]$ and $y_{T_{pe}}[i]$ series obtained from SL (red) and ML (blue) delineation for a particular subject from the database. Dashed lines mark the start and end of the tilt.

The time required for "s" to complete 90% of its rate adaptation, denoted by $t_{90}$, is computed by setting a threshold of 0.1 to the cumulative sum of the estimated filter impulse response, denoted by $c[j]$:

$$c[j] = \sum_{l=j}^{N} h[l], \quad j = 1, ..., N \qquad (6)$$

leading to

$$t_{90} = \frac{1}{F_m} \arg \max_{j} (c[j] > 0.1), \quad j = 1, ..., N \qquad (7)$$

Other indices describing the time required to complete 25, 50 and 70% of rate adaptation, denoted by $t_{25}$, $t_{50}$ and $t_{70}$, were calculated analogously.

## 3. Results and discussion

### 3.1. QT interval dynamics

The QT interval responded to abrupt RR changes following an exponential adaptation in all the analyzed subjects. An example of that adaptation is illustrated in Fig. 2 for a particular subject of the investigated database. As can be seen from Fig. 2, QT dynamics are very similar when calculated using SL or ML delineation techniques.

To quantify the time required for QT to complete its rate adaptation, $t_{90}$, $t_{70}$, $t_{50}$ and $t_{25}$ indices were measured. The results obtained from SL and ML series are shown in Table 1. No significant differences were observed between QT adaptation times calculated using SL or ML delineation.

### 3.2. $T_{pe}$ interval dynamics

The $T_{pe}$ interval responded to abrupt RR changes in a rapid way for $y_{T_{pe}}^{\text{SL}}[i]$ series, but more steadily for $y_{T_{pe}}^{\text{ML}}[i]$ series, as illustrated in Fig. 2. This effect is reflected in the rate adaptation times shown in Table 1, where significant differences are observed when comparing SL and ML

Table 1. Mean $\pm$ standard deviation across all subjects of the times required to complete 90% ($t_{90}$), 70% ($t_{70}$), 50% ($t_{50}$) and 25% ($t_{25}$) of rate adaptation for both SL and ML delineation techniques. In the right column, p-values obtained from a Student's t-test.

|  | $QT^{\text{SL}}$ | $QT^{\text{ML}}$ | p-value |
|---|---|---|---|
| $t_{90}[s]$ | $49.7 \pm 29.0$ | $47.1 \pm 20.1$ | 0.305 |
| $t_{70}[s]$ | $32.1 \pm 16.2$ | $24.9 \pm 12.1$ | 0.152 |
| $t_{50}[s]$ | $15.9 \pm 9.4$ | $13.1 \pm 10.7$ | 0.143 |
| $t_{25}[s]$ | $3.6 \pm 2.6$ | $4.3 \pm 5$ | 0.309 |
|  | $T_{pe}^{\text{SL}}$ | $T_{pe}^{\text{ML}}$ | p-value |
| $t_{90}[s]$ | $25.6 \pm 37.3$ | $56.4 \pm 48.3$ | 0.012 |
| $t_{70}[s]$ | $13.9 \pm 21.9$ | $37.5 \pm 37.4$ | 0.010 |
| $t_{50}[s]$ | $6.9 \pm 12.1$ | $19.5 \pm 25.7$ | 0.029 |
| $t_{25}[s]$ | $1.8 \pm 2.8$ | $6.9 \pm 14.2$ | 0.092 |

delineation techniques. As $y_{\text{QT}}^{\text{SL}}[i]$ and $y_{\text{QT}}^{\text{ML}}[i]$ rate adaptations are similar, it can be postulated that dissimilarities between $y_{T_{pe}}^{\text{SL}}[i]$ and $y_{T_{pe}}^{\text{ML}}[i]$ series adaptations arise from the fact that differences in T-wave peak delineation between the two methods do not parallel differences in T-wave end delineation.

Fig. 3 shows three different T-wave loops at time instants *pre* (before the tilt is started), *dur* (during the tilt) and *pos* (when the tilt has already finished) marked on $y_{T_c'}[i]$ series calculated for the same subject whose QT and $T_{pe}$ series are shown in Fig. 2. Blue axis indicates ML optimum projection direction for peak delineation, black axis indicates ML optimum projection direction for offset delineation and red axis shows SL direction. Likewise, blue and red dots represent ML and SL T-wave peak marks, respectively, and blue and red stars represent ML and SL T-wave offset marks.
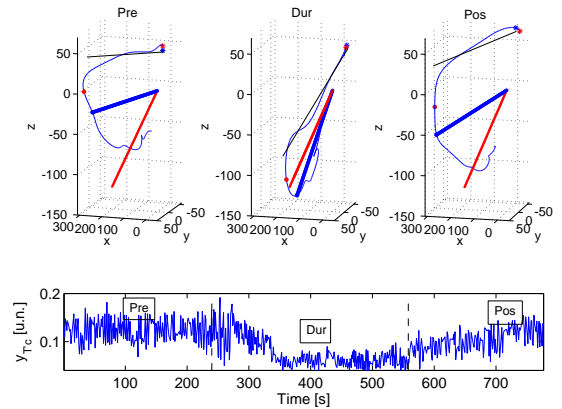


Figure 3. Top panels: T-wave loops at time instants *pre* (before the tilt starts), *dur* (during the tilt) and *pos* (after the tilt). Blue and black axis indicate ML optimum projection direction for peak and offset delineation, respectively and red axis shows SL direction. Bottom panel: $y_{T_c'}[i]$ series.
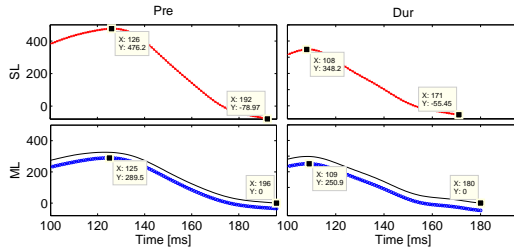
675

Figure 4. T-wave peak and offset marks at time instants *pre* and *dur* delineated over the SL lead (above), the optimum projected lead for peak delineation (below, blue) and the optimum projected lead for offset delineation (below, black).

When comparing the loops between instants *pre* or *pos* and *dur*, it can be seen that blue and black axis follow the loop's rotation produced by the postural change. This postural change also modifies the morphology of the loop, as $y_{T_c'}$[i] series shows in Fig. 3, therefore varying the projected waves in a significant way from *pre* to *dur* or from *dur* to *pos* (the former case can be seen in Fig. 4), affecting T-peak and T-offset delineation marks and, therefore, $T_{pe}$ measure. ML takes the peak mark from the wave obtained from blue axis (Fig. 4, below, blue) and the offset mark from the wave obtained from black axis (Fig. 4, below, black), which will always be later than the one from SL delineation, and the distance between these two marks is approximately maintained along the record.

SL, on the contrary, keeps the same projection direction all over the record, and thus peak and offset marks are both delineated over the same wave. $T_{pe}$ computation will be then affected by the rotation induced by the postural change.

## 4.    Conclusions

QT and $T_{pe}$ intervals, as well as their rate dependence, have been proposed as arrythmic risk stratifiers. However, the delineation method used for their evaluation must be carefully considered and analyzed in order to properly interpret the results. As shown in this study, QT rate adaptation does not differ when using SL or ML delineation. $T_{pe}$ rate adaptation, however, is very sensitive to the delineation method. ML delineation follows electric heart axis movement to remove the postural change effect, producing $T_{pe}$ series accounting only for electrical sources and so of flatter rate dependence than those obtained from SL delineation, which are also affected by T-wave loop rotation. Additionally, the ML delineation provides series with higher variance, possibly as a result of the beat-to-beat adjustment to the optimum projection, which could generate some series instability and artifacted larger adaptation time. QT series are not very much affected by the delineation method because delineation of wave onsets and offsets is not that sensitive to loop rotations.

## References

[1] Coumel P, Fayn J, Maison-Blanche P, Rubel P. Clinical relevance of assessing QT dynamicity in holter recordings. Journal of Electrocardiology 1994;27:62–66.

[2] Couderc JP, Zhou M, Sarapa N, Zareba W. Investigating the effect of sotalol on the repolarization intervals in healthy young individuals. Journal of Electrocardiology 2008;41:595–602.

[3] Yamaguchi M, Shimizu M, Ino H, Terai H, Uchiyama K, Oe K, Mabuchi T, Konno T, Kaneda T, Mabuchi H. T wave peak-to-end interval and QT dispersion in acquired long QT syndrome: a new index for arrythmogenicity. Clinical Science 2003;105:671–676.

[4] Antzelevitch C, Viskin S, Shimizu W, Yan GX, Kowey P, Zhang L, Sicouri S, Diego JMD, Burashnikov A. Does Tpeak-Tend provide an index of transmural dispersion of repolarization? Heart Rhythm 2007;4(8):1114–1119.

[5] Browne K, Zipes D, Heger J, Prystowsky E. Influence of the autonomic nervous system on the QT interval in man. American Journal of Cardiology 1982;50:1099–1103.

[6] Mincholé A, Pueyo E, Rodríguez JF, Zacur E, Doblaré M, Laguna P. Quantification of Restitution Dispersion From the Dynamic Changes of the T-wave Peak to End, Measured at the Surface ECG. IEEE Transactions on Biomedical Engineering May 2011;58(5):1172–1182.

[7] Pueyo E, Smetana P, Caminal P, Bayes, Malik M, Laguna P. Characterization of QT interval adaptation to RR interval changes and its use as a risk-stratifier of arrythmic mortality in amiodarone-treated survivors of acute myocardial infarction. IEEE Transactions on Biomedical Engineering 2004; 51(9):1511–1520.

[8] Almeida R, Martínez JP, Rocha AP, Laguna P. Multilead ECG delineation using spatially projected leads from wavelet transform loops. IEEE Transactions on Biomedical Engineering 2009;56:1996–2005.

[9] Priori S, Mortara D, Napolitano C, Diehl L, Paganini V, Cantù F, Cantú G, Schwartz P. Evaluation of the spatial aspects of T wave complexity in the long-QT syndrome. Circulation 1997;96:3006–3012.

[10] Okin P, Devereux R, Lee E, Galloway J, Howard B. Electrocardiographic repolarization complexity and abnormality predict all-cause and cardiovascular mortality in diabetes. The Strong Heart Study 2004;53:434–440.

Address for correspondence:

Julia Ramírez García
I3A, Edificio I+D+i, Mariano Esquillor s/n, Zaragoza
Julia.Ramirez@unizar.es